28 May 2010, 2:00 pm - 3:30 pm

Calibration of Soil Amplification Factors for Real-Time Ground-Motion Scenarios in Italy

Simone Barani
University of Genoa, Italy

Roberto De Ferrari
University of Genoa, Italy

Gabriele Ferretti
University of Genoa, Italy

Daniele Spallarossa
University of Genoa, Italy


Fifth International Conference on
Recent Advances in Geotechnical Earthquake Engineering and Soil Dynamics
and Symposium in Honor of Professor I.M. Idriss
May 24-29, 2010 • San Diego, California

CALIBRATION OF SOIL AMPLIFICATION FACTORS FOR REAL-TIME GROUND-MOTION SCENARIOS IN ITALY

Simone Barani
Dip.Te.Ris.
University of Genoa
Viale Benedetto XV
16132 Genoa, Italy

Roberto De Ferrari
Dip.Te.Ris.
University of Genoa
Viale Benedetto XV
16132 Genoa, Italy

Gabriele Ferretti
Dip.Te.Ris.
University of Genoa
Viale Benedetto XV
16132 Genoa, Italy

Daniele Spallarossa
Dip.Te.Ris.
University of Genoa
Viale Benedetto XV
16132 Genoa, Italy

ABSTRACT

This study deals with the calibration of soil amplification factors to be used for generating site-specific, real-time (or quasi real-time) ground-motion scenarios in Italy. To this end, the ground response of 100 soil profiles is studied through 1-dimensional (1D) equivalent-linear numerical simulations. Several real, rock ground-motion time histories, grouped into different peak ground acceleration (PGA) classes, are driven through the models of the soil columns. Soil amplification factors are then calculated using different definitions, either as the ratio of the spectral acceleration at the surface to the spectral acceleration at the rock outcrop or by dividing the (acceleration or pseudo-velocity) response spectrum intensity at the surface to the reference response spectrum intensity. Finally, regression analyses are performed to derive empirical equations that relate the amplification factor to different soil parameters, such as the average shear wave velocity $V_{S,30}$ in the top 30 m of a soil profile and the soil fundamental frequency, f_0. The reliability of the amplification factors here calculated is verified through comparison with experimental data recorded during the April 6, 2009 L'Aquila earthquake (M_w = 6.3).

INTRODUCTION

Producing ground shaking scenarios immediately following seismic events has become common practice in seismological research centers in the last decade. These maps, which are made available within a few minutes of an earthquake via the Web or dedicated communications, are useful for public and scientific consumption and, most important, for planning emergency response, recovery strategies, and humanitarian assistance in case of destructive events.

Nowadays, most seismological centers produce shaking maps using ShakeMap® (Wald et al., 2003; http://earthquake.usgs.gov/shakemap), a software which has been adopted as a standard tool by the worldwide scientific community. Basically, this software combines instrumental measurements of shaking with information about local geology and earthquake location and magnitude to evaluate shaking distribution within an area. As such, "*shaking maps presents a rapid portrayal of the extent of potentially damaging shaking following an earthquake*" (Wald et al., 2006). The reliability of these maps depends on several factors, such as the ground-motion predictive equation used to estimate the attenuation of the shaking level as a function of magnitude and distance, the geological model adopted to provide an estimation of the average shear wave velocity $V_{S,30}$ in the upper 30 m, and site correction factors adopted to account for amplification effects produced by particular soil conditions.

This paper, which has been developed within the framework of the 2007-2009 DPC-INGV S3 Project, deals with the calibration of soil amplification factors (or soil coefficients) for producing real-time (or quasi real-time) ground-motion scenarios in Italy using ShakeMap®. Since this software has been adopted as reference tool for automatic generation of shaking maps in Italy (about five years ago), ground-motion amplitude predicted on rock is corrected by applying the NEHRP soil coefficients (Building Seismic Safety Council – BSSC, 2003), which were derived from both empirical and numerical studies following the 1989 Loma Prieta earthquake (Borcherdt, 1994). Therefore, it seems appropriate to estimate specific amplification factors based on an Italian database of soil profiles.

The study can be summarized as follows. First a large number of real accelerograms recorded at rock sites were selected from different national and international databanks and, then, were grouped into different peak ground acceleration (PGA) classes. Contemporaneously, geotechnical and geophysical data relevant at a hundred of soil profiles with different characteristics were collected in order to define 1-dimensional (1D) soil models. Then, accelerograms were driven through these models to evaluate their response via equivalent-linear analyses. Finally, the level of amplification, defined as the ratio of the ground-motion intensity (quantified either in terms of spectral acceleration or in terms response spectrum intensity) at the surface to the reference motion at the rock outcrop, was related to $V_{S,30}$ and the soil fundamental frequency, f_0. Although an f_0 map is still not available for all of Italy but only for a number of municipalities, predictive equations that relate the amplification factor to both $V_{S,30}$ and f_0 are derived for future implementation in ShakeMap®. The use of f_0 in conjunction with $V_{S,30}$, indeed, is strongly recommended by several authors (e.g., Pitilakis et al. 2006, Barani et al., 2008) showing that the fundamental soil frequency is more effective than $V_{S,30}$ in predicting the soil amplification.

GROUND-MOTION DATA SET

The ground-motion data set on which ground response analyses are based consists of 240 triaxial recordings from 80 worldwide weak and strong earthquakes ($2.5 \leq M \leq 7.9$). These recordings were selected from a larger data set including more than 1400 accelerograms recorded at sites classified as "rock". Here, the term "rock" refers to sites with $V_{S,30}$ greater than 800 m/s, accordingly to the classification proposed by the Italian building code (Ministero delle Infrastrutture e dei Trasporti, 2008).
Recordings were downloaded from the following databanks based exclusively on their PGA value:

- ITACA – Italian Accelerometric Archive (Working Group ITACA, 2008)
- ESD – European Strong Motion Database (Ambraseys et al., 2002)
- PEER NGA database (http://peer.berkeley.edu/nga/)
- K-net – Kyoshin Network (http://www.k-net.bosai.go.jp/)

A careful revision was considered to be necessary as the data come from a variety of sources of different accuracy and reliability. In particular, time histories presenting consecutive earthquakes or possible saturation effects were excluded from the data set. Moreover, horizontal to vertical (H/V) spectral ratios were calculated to verify the reliability of site classification. Another criterion adopted in the selection of accelerograms was the location of earthquakes. In particular, priority was given to Italian and European data. This reduced the full data set to 80 events that are listed in Table 1. For each event, only the horizontal component with the highest PGA value was used in the numerical simulations.
The selected accelerograms were classified into five PGA categories: 1) PGA ≤ 0.05 g, 2) 0.05 g < PGA ≤ 0.15 g, 3) 0.15 g < PGA ≤ 0.25 g, 4) 0.25 g < PGA ≤ 0.35 g, 5) PGA > 0.35 g. PGA values ranges from approximately 0.015 g to 0.58 g, compatible with the Italian seismicity and the reference PGA hazard values corresponding to mean return periods up to 2475 years (Gruppo di Lavoro MPS, 2004; Meletti and Montaldo 2007). According to Bazzurro and Cornell (2004), a minimum number of 10 records were selected for each PGA class. Specifically, 20 accelerograms were selected for each one of the first three classes while 10 records were considered for the remaining two. The distribution of recordings with respect to magnitude, M, source-to-site distance (expressed in terms of epicentral distance, R), and PGA classification is shown in Fig. 1.

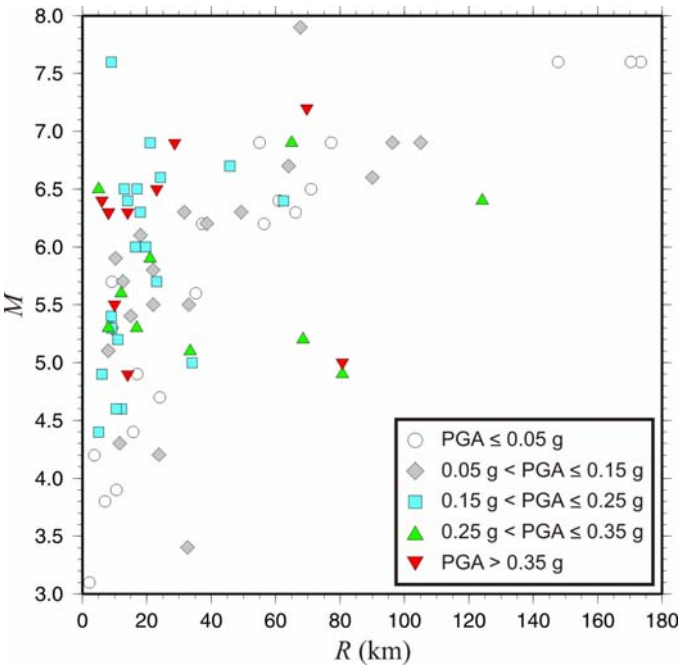

Fig. 1. Distribution of M and R values included in the ground-motion database.

SOIL MODELING

In order to calibrate empirical equations to predict the soil amplification as a function of $V_{S,30}$, the seismic response of 100 soil profiles, defined by several geotechnical and geophysical data and representing different soil conditions, is studied through 1D numerical simulations. Given the limited availability of complete geophysical and geotechnical data necessary to define accurate models of the soil columns, our present data set collects profiles from four Italian regions only: Molise, Tuscany, Abruzzo, and Piedmont. The data set will be continuously updated as well as the amplification factor values.

Table 1. List of ground-motion records used in numerical simulations.

Earthquake #	Earquake Name	Earthquake Country	Date	Epicentre Lat	Epicentre Lon	*M*	*R* (km)	Station Code	PGA (g)	Databank
1	San Fernando	California	09/02/1971	34.44	-118.41	6.6	24.2	L04	0.192	PEER
2	Friuli	Italy	06/05/1976	46.29	13.25	6.5	23.0	TLM1	0.357	ESD
3	Friuli (3rd shock)	Italy	15/09/1976	46.30	13.19	6.1	18.0	SRC0	0.138	ITACA
4	Friuli (4th shock)	Italy	15/09/1976	46.30	13.18	6.0	16.4	SRC0	0.249	ITACA
5	Friuli	Italy	16/09/1976	46.28	12.98	5.3	9.1	SMT	0.100	ITACA
6	Friuli	Italy	16/09/1977	46.28	12.98	5.3	9.1	SMU	0.181	ITACA
7	Friuli (aftershock)	Italy	16/09/1977	46.28	12.98	5.4	9.0	SMU	0.191	ESD
8	Patti Gulf	Italy	15/04/1978	38.27	15.11	5.5	33.0	NAS	0.149	ITACA
9	Montenegro	Serbia & Montenegro	09/04/1979	41.95	19.04	5.4	15.0	ULA	0.061	ESD
10	Montenegro	Serbia & Montenegro	15/04/1979	41.98	18.98	6.9	55.0	TIS	0.031	ESD
11	Montenegro	Serbia & Montenegro	15/04/1979	41.98	18.98	6.9	105.0	DUB	0.075	ESD
12	Montenegro (aftershock)	Serbia & Montenegro	15/04/1979	42.29	18.68	5.8	22.0	HRZ	0.093	ESD
13	Montenegro	Serbia & Montenegro	15/04/1979	41.98	18.98	6.9	21.0	ULA	0.224	ESD
14	Montenegro	Serbia & Montenegro	15/04/1979	41.98	18.98	6.9	65.0	HRZ	0.256	ESD
15	Montenegro (aftershock)	Serbia & Montenegro	17/04/1979	42.46	18.62	5.1	8.0	HRZ	0.056	ESD
16	Coyote Lake	California	06/08/1979	37.08	-121.51	5.7	12.6	G01	0.132	PEER
17	Garfagnana	Italy	07/06/1980	44.05	10.60	4.3	11.5	BRG	0.061	ITACA
18	Irpinia	Italy	23/11/1980	40.85	15.33	6.2	37.2	A-ARI	0.023	PEER
19	Irpinia	Italy	23/11/1980	40.81	15.34	6.9	77.2	B-AUL	0.042	PEER
20	-	Italy	16/01/1981	40.78	15.35	3.9	10.6	CNB	0.040	ITACA
21	-	Italy	16/01/1981	40.84	10.5E	4.6	10.5	CR2	0.151	ITACA
22	-	Italy	16/01/1981	40.84	10.50	4.6	12.1	CR3	0.169	ITACA
23	Campano Lucano (aftershock)	Italy	14/02/1981	41.00	14.67	4.9	17.0	ARN	0.029	ESD
24	-	Italy	20/09/1981	42.96	12.98	2.5	31.5	SPL	0.033	ITACA
25	-	Italy	18/09/1982	38.37	14.97	3.4	32.7	NAS	0.079	ITACA
26	Morgan Hill	California	24/04/1984	37.31	-121.70	6.2	38.6	G01	0.098	PEER
27	Al Comino	Italy	07/05/1984	41.70	13.86	5.9	10.3	ATN	0.112	ITACA
28	Val Comino	Italy	11/05/1984	41.78	13.89	5.7	9.1	PSC	0.020	ITACA
29	Massiccio Meta	Italy	01/07/1984	41.73	13.95	4.4	15.8	PSC	0.020	ITACA
30	Garfagnana	Italy	23/01/1985	44.06	10.41	4.2	3.7	BRG	0.043	ITACA
31	Whittier Narrows	California	01/10/1987	34.05	-118.08	6.0	19.6	A-MTW	0.186	PEER
32	SE of Appricena	Italy	11/03/1989	41.85	15.49	3.8	7.0	SNN	0.044	ESD
33	Loma Prieta	California	18/10/1989	37.04	-121.88	6.9	96.3	PHT	0.061	PEER
34	Loma Prieta	California	18/10/1989	37.04	-121.88	6.9	28.6	G01	0.473	PEER
35	Northridge	California	17/01/1994	34.21	-118.55	6.7	64.0	ATB	0.068	PEER
36	Northridge	California	17/01/1994	34.21	-118.55	6.7	45.8	MTW	0.234	PEER
37	Firuzabad	Iran	20/06/1994	29.01	52.64	5.9	21.0	ZRT	0.310	ESD
38	Kozani	Greece	13/05/1995	40.18	21.66	6.5	71.0	FLO	0.026	ESD
39	Kozani	Greece	13/05/1995	40.18	21.66	6.5	17.0	KOZ	0.208	ESD
40	-	Tōhoku (offshore)	23/05/1996	38.65	142.31	5.0	80.7	MYG	0.579	K-NET
41	Mt. Hengill Area	Iceland	24/08/1997	64.04	-21.27	4.9	6.0	102	0.172	ESD
42	Umbria-Marche	Italy	26/09/1997	43.02	12.89	5.6	35.2	CSC	0.030	ITACA
43	Umbria Marche	Italy	26/09/1997	40.02	12.89	5.7	23.0	CTR	0.183	ESD
44	Umbria Marche (aftershock)	Italy	03/10/1997	43.00	12.84	5.3	8.0	NCB	0.284	ESD
45	Umbria Marche (aftershock)	Italy	06/10/1997	43.02	12.84	5.5	10.0	NCB	0.361	ESD
46	Umbria Marche (aftershock)	Italy	12/10/1997	42.91	12.95	5.2	11.0	CTR	0.156	ESD
47	Kalamata	Greece	13/10/1997	36.38	22.07	6.4	61.0	GHI	0.021	ESD
48	Umbria-Marche (3rd shock)	Italy	14/10/1997	42.90	12.90	5.5	22.0	CSC	0.061	ITACA
49	Umbria Marche (aftershock)	Italy	14/10/1997	42.92	12.93	5.6	12.0	CTR	0.337	ESD
50	NW of Makrakomi	Greece	21/10/1997	38.97	22.07	4.7	24.0	KRP	0.015	ESD
51	Strofades	Greece	18/11/1997	37.48	20.69	6.6	90.0	KYP	0.074	ESD
52	-	Tōhoku (offshore)	07/12/1997	37.72	141.78	5.2	68.5	MYG	0.277	K-NET
53	Appennino Umbro-Marchigiano	Italy	12/01/1998	43.01	12.88	3.1	2.2	CESM	0.020	ITACA
54	Oelfus	Iceland	14/11/1998	63.96	-21.24	4.4	5.0	102	0.236	ESD
55	-	Tōhoku (offshore)	24/11/1998	38.00	141.58	5.1	33.4	MYG	0.293	K-NET
56	Monti Nebrodi	Italy	14/02/1999	38.23	15.02	4.2	23.8	NAS	0.066	ITACA
57	Izmit	Turkey	17/08/1999	40.70	29.99	7.6	9.0	IZT	0.228	ESD
58	Chi-Chi	Taiwan	20/09/1999	23.86	120.80	7.6	147.7	KAU003	0.020	PEER
59	Chi-Chi	Taiwan	20/09/1999	23.86	120.80	7.6	170.3	TAP065	0.036	PEER
60	Chi-Chi	Taiwan	20/09/1999	23.86	120.80	7.6	173.4	TAP077	0.040	PEER
61	Chi-Chi	Taiwan	22/09/1999	23.81	121.08	6.2	56.4	HWA003	0.025	PEER
62	Chi-Chi	Taiwan	25/09/1999	23.87	121.01	6.3	66.2	HWA003	0.038	PEER
63	Izmit (aftershock)	Turkey	07/11/1999	40.70	30.72	4.9	14.0	C0375	0.352	ESD
64	-	Tōhoku (offshore)	20/03/2000	37.99	141.50	5.0	34.1	MYG	0.202	K-NET
65	South Iceland	Iceland	17/06/2000	63.97	-20.36	6.5	13.0	108	0.156	ESD
66	South Iceland (aftershock)	Iceland	17/06/2000	63.97	-20.36	6.5	5.0	106	0.338	ESD
67	South Iceland (aftershock)	Iceland	21/06/2000	63.97	-20.71	6.4	14.0	101	0.178	ESD
68	South Iceland (aftershock)	Iceland	21/06/2000	63.97	-20.71	6.4	6.0	107	0.568	ESD
69	-	Chūgoku	24/03/2001	34.12	132.71	6.4	62.4	YMG	0.159	K-NET
70	-	Tōhoku	02/12/2001	39.40	141.26	6.4	124.1	MYG	0.278	K-NET
71	Denali	Alaska	03/11/2002	63.54	-147.44	7.9	67.7	5595	0.100	PEER
72	-	Tōhoku (offshore)	05/12/2002	38.72	142.26	4.9	80.7	MYG	0.259	K-NET
73	Bingol	Turkey	01/05/2003	39.01	40.51	6.3	14.0	BIN	0.515	ESD
74	-	Tōhoku (offshore)	16/08/2005	38.15	142.28	7.2	69.7	MYG	0.509	K-NET
75	Olfus	Iceland	29/05/2008	64.01	-21.01	6.3	8.0	112	0.509	ESD
76	Olfus	Iceland	29/05/2008	64.01	-21.01	6.3	8.0	101	0.536	ESD
77	L'Aquila	Italy	06/04/2009	42.33	13.33	6.3	49.3	CLN	0.066	ITACA
78	L'Aquila	Italy	06/04/2009	42.33	13.33	6.3	31.6	ORC	0.091	ITACA
79	L'Aquila	Italy	06/04/2009	42.33	13.33	6.3	18.0	GSA	0.151	ITACA
80	L'Aquila	Italy	07/04/2009	42.27	13.46	5.3	16.8	GSA	0.282	ITACA

Physical and mechanical parameter values (e.g., shear wave velocity, unit weight, shear strength modulus, etc.) used to define 1D soil models were derived from both laboratory tests and field geophysical investigations (e.g., boreholes, penetrometric tests, downhole tests, H/V measurements, and seismic refraction profiles). Only the ground response of those profiles for which it was possible to define the depth and properties of bedrock (i.e., infinite half-space at the bottom of a soil profile) is analyzed in this study. Except for soil profiles in Molise, which are generally characterized by a flyschoid intensely fractured soft bedrock (Roure et al., 1991) with mean shear wave velocity, V_S, as low as approximately 690 m/s, we assume as bedrock those materials with V_S greater than or equal to 800 m/s. Substantial differences in bedrock stiffness are due to the different geological setting and tectono-dynamic evolution of the areas considered.

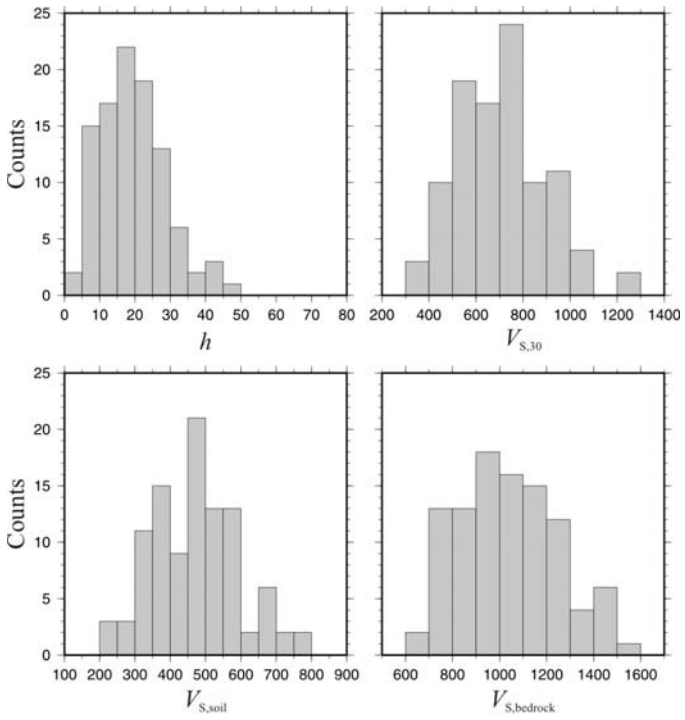

Fig. 2. Histograms summarizing the main characteristics of the soil profile data set.

Figure 2 summarizes the main characteristics of the soil model data set. Altogether, the thickness, h, of soil deposits (measured from the top of the bedrock to the surface) ranges between 4 and 48 m, the average shear wave velocity of the top 30 m, $V_{S,30}$, between 369 and 1227 m/s, the mean shear wave velocity of soil deposits, $V_{S,soil}$, between 200 and 796 m/s, and the shear wave velocity of bedrock, $V_{S,bedrock}$, between 690 and 1500 m/s. It should be observed that most sites considered in this study present a rather shallow soil deposit above the bedrock, which is usually less than 30 m deep. In only 10% of cases, indeed, the bedrock is deeper than 30 m. Note, finally, that our data set lacks of type C and D[1] profiles. Only a small number of type C and D profiles were collected but they were not included in the final data set since located in deep alluvial basins. In these cases, the assumption of horizontal material boundaries required for a correct use of a 1D analysis is violated and, consequently, 2D simulations should be performed.

NUMERICAL SIMULATIONS

1D ground response analyses were carried out using Shake91 (Schnabel et al., 1972; Idriss and Sun, 1993), a computer program that uses an iterative, equivalent-linear approach to approximate the nonlinear, inelastic behavior of soils. This program computes the response of a soil deposit that is idealized as a system of homogeneous visco-elastic layers of infinite horizontal extent overlying a uniform half-space (bedrock) subjected to vertically propagating shear waves. In order to consider the nonlinear behavior of materials under dynamic conditions, modulus reduction and damping curves are required in input. Except for some materials in Tuscany, whose dynamic properties were evaluated from specific laboratory tests (Foti et al., 2002), modulus reduction and damping curves were derived from scientific literature (e.g., Seed and Idriss, 1970; Seed et al., 1986; Sun et al., 1988). Specifically, they were selected based on the granulometry, plasticity index, and relative density of materials.

Figure 3 compares the average (average over the n accelerograms applied as input motion at the base of each soil column) amplification functions, $AF(f)$, and 5%-damped surface response spectra obtained for input motions with 0.05 g < PGA ≤ 0.15 g (Fig. 3a) and PGA > 0.35 g. (Fig. 3b). Note how the nonlinear behavior of soils subjected to stronger motions (Fig. 3b) corresponds to a general decrease in the amplitude of the resonant peaks that tend to be shifted towards lower frequencies.

EVALUATION OF SOIL AMPLIFICATION FACTORS

Soil amplification factors are calculated using three different definitions. The first calculates the amplification factor as the ratio of the acceleration spectrum intensity at the surface, ASI^S, to the acceleration spectrum intensity at the rock outcrop, ASI^R:

[1] The site classification proposed by the Italian building code (Ministero delle Infrastrutture e dei Trasporti, 2008) defines five soil categories: Class A corresponds to rock sites ($V_{S,30}$ > 800 m/s), Site B to soft rock, very dense and stiff soils (180 m/s < $V_{S,30}$ ≤ 360 m/s), Class C to dense or medium-dense soils (180 m/s < $V_{S,30}$ ≤ 350 m/s), Class D to loose-to-medium cohesionless soil ($V_{S,30}$ ≤ 180 m/s), and Class E to soil profiles consisting of a surface alluvium layer with $V_{S,30}$ values of type C or D and thickness up to 20 m, underlain by stiffer material with $V_{S,30}$ > 800 m/s.

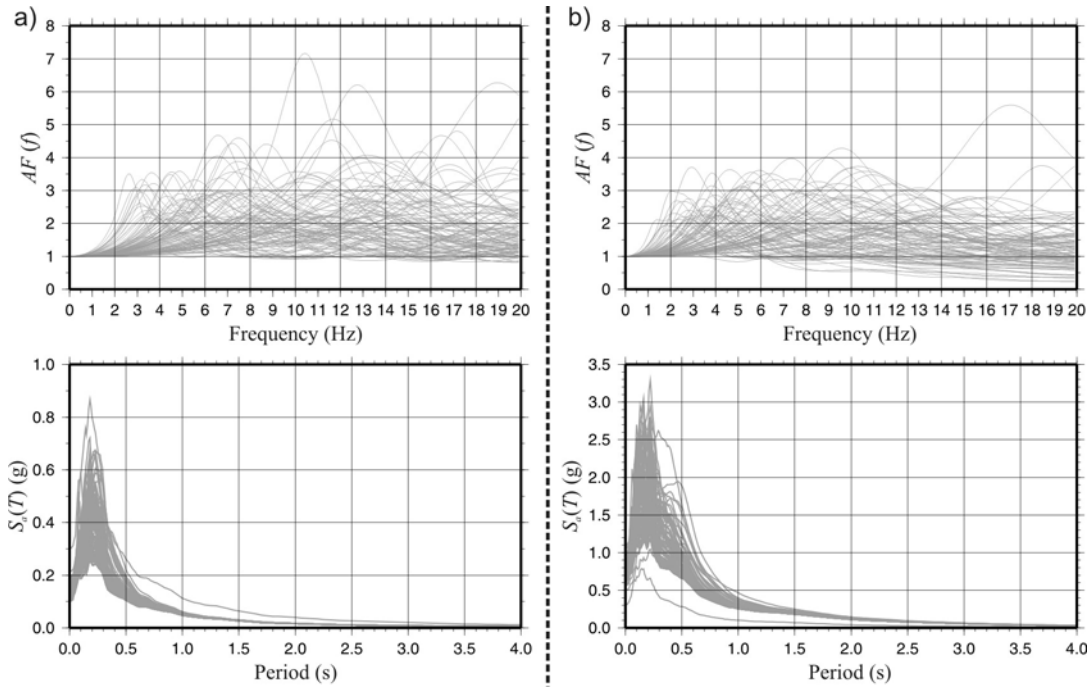

Fig. 3. Amplification functions, AF(f), and surface response spectra, $S_a(T)$, obtained for input motions with 0.05 g < PGA ≤ 0.15 g (a) and PGA > 0.35g.

$$Fa = \frac{ASI^S}{ASI^R} \tag{1}$$

The acceleration spectrum intensity is calculated as proposed by Rey et al. (2002) for estimating the site factors included in the Eurocode 8 – EC8 (Comitè Europèen de Normalisation – CEN, 2003):

$$ASI = \int_{0.05}^{2.5} S_a(T)dT \tag{2}$$

where $S_a(T)$ indicates the 5%-damped spectral acceleration and T is the spectral period.
In the second definition, distinction is made between short- (i.e., $T \leq 0.5$ s) and long- (i.e., $T > 0.5$ s) period motions:

$$\begin{cases} Ca = \dfrac{ASI^S}{ASI^R} & T \leq 0.5\text{s} \\ Cv = \dfrac{SI^S}{SI^R} & T > 0.5\text{s} \end{cases} \tag{3}$$

where the acceleration spectrum intensity is calculated using Eq. 2 but assuming $T = 0.1$ s and $T = 0.5$ s as integration limits (Von Thun et al., 1988) and SI is the 5%-damped pseudo-velocity response spectrum intensity (Housner, 1952):

$$SI = \int_{0.1}^{2.5} PSV(T)dT \tag{4}$$

Makdisi and Seed (1978) suggested the use of the pseudo-velocity response spectrum intensity for evaluation of the response of structures with fundamental periods between 0.6 and 2.0 s while the acceleration response spectrum intensity calculated between 0.1 and 0.5 s was suggested to characterize strong ground-motion for analyses of structures with fundamental periods of less than 0.5 s (Von Thun et al., 1988). Thirdly, a frequency-dependent amplification factor is calculated as the ratio of the spectral acceleration at the surface, $S_a^S(T)$, to the spectral acceleration at the rock outcrop, $S_a^R(T)$ (e.g., Bazzurro and Cornell, 2004; Choi and Stewart, 2005):

$$SR(T) = \frac{S_a^S(T)}{S_a^R(T)} \tag{5}$$

For each soil model, n amplification factor values are calculated, where n indicates the number of records used in the dynamic analysis. These values are then averaged and the mean and standard deviation are determined.

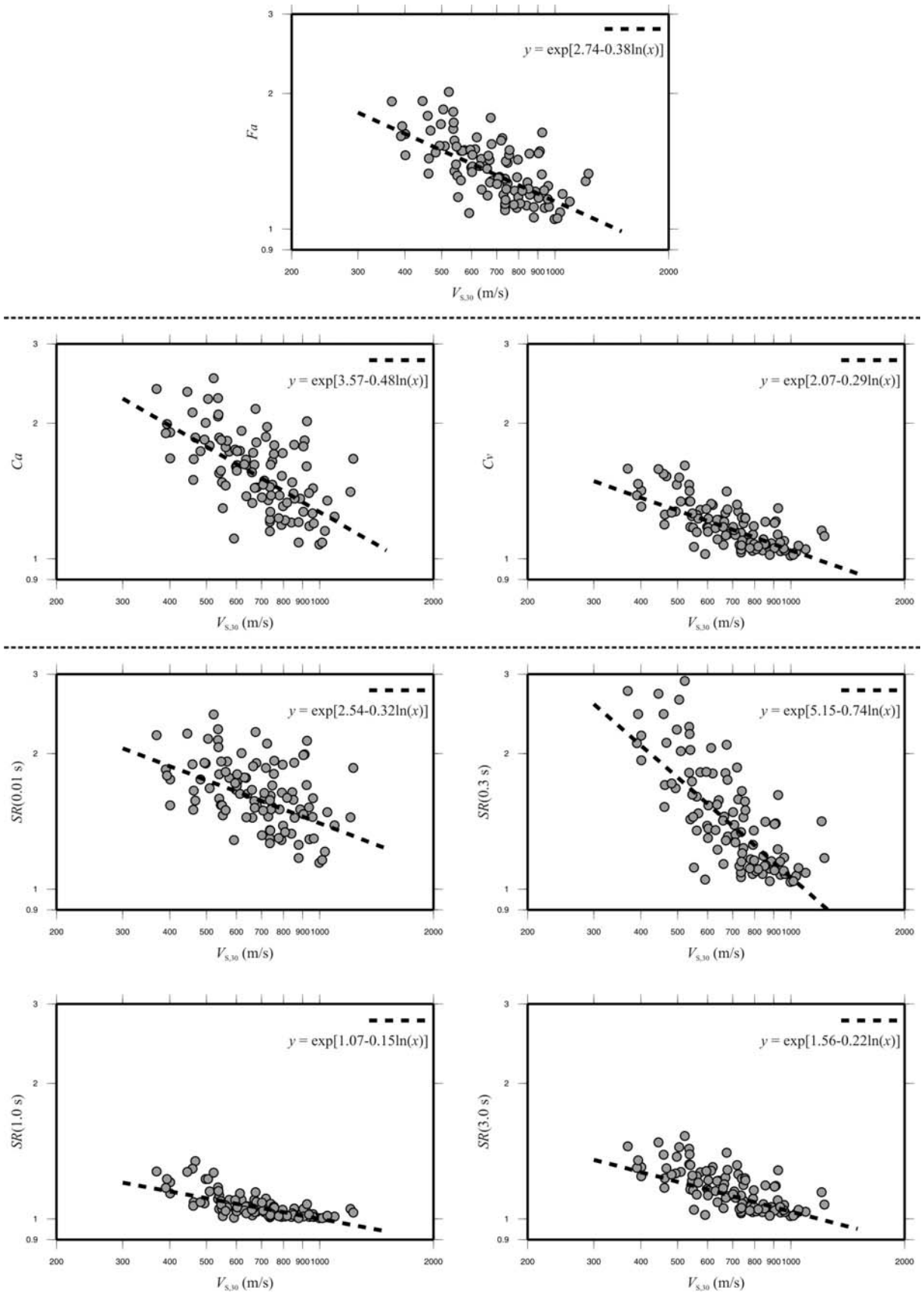

Fig. 4. Average amplification factors and regression curves for input motions with 0.05 g < PGA ≤ 0.15 g.

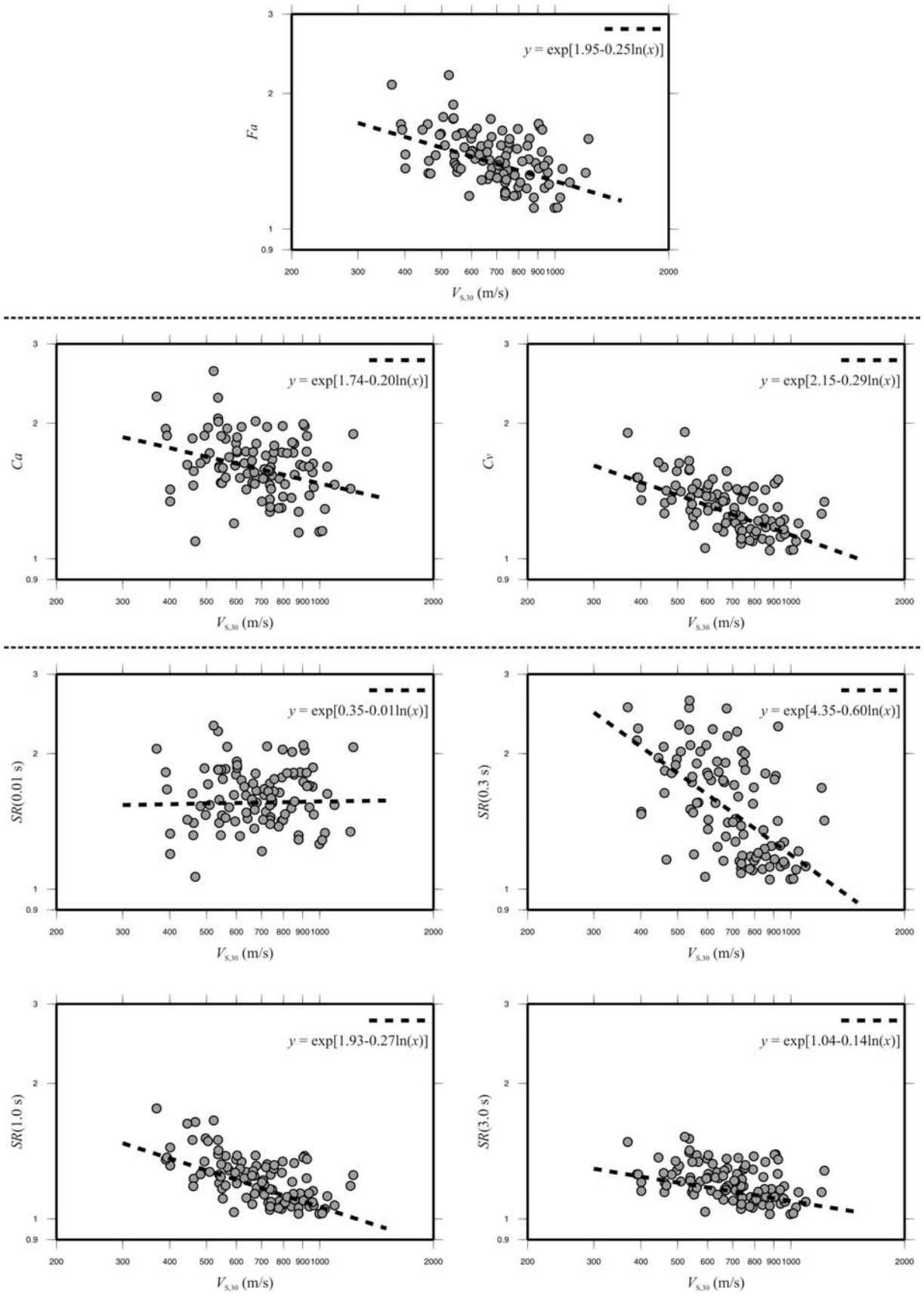

Fig. 5. Average amplification factors and regression curves for input motions with PGA > 0.35 g.

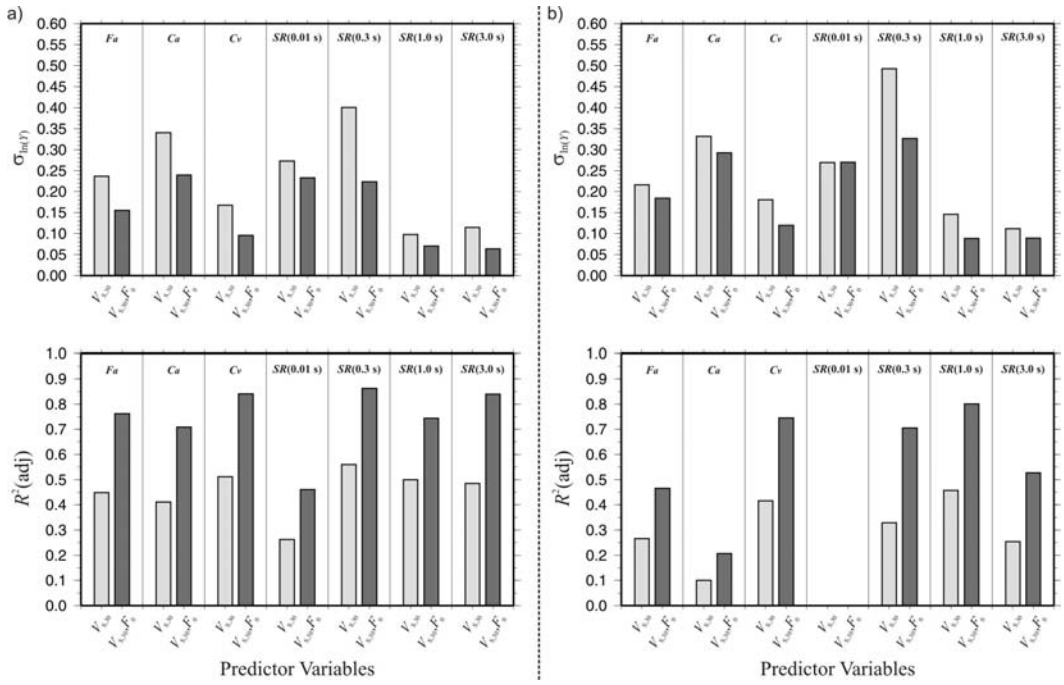

Fig. 6. Values of the residual standard deviation, $\sigma_{\ln(Y)}$, and coefficient of multiple determination, R^2(adj), obtained from single and multiple regression models for input motions with 0.05g < PGA ≤ 0.15 g (a) and PGA > 0.35 g (b).

In order to define empirical predictive equations that relate the level of amplification to $V_{S,30}$, regression analyses were performed using a weighted least mean square algorithm. This regression method has the advantage that allows for response data of different quality. Thus, it was possible to account for the uncertainty in the amplification factor values due to the uncertainty in the ground-motion recordings. Given the amplification factor variance, weights are simply estimated as the reciprocal of the variance. An analogous multiple regression algorithm was used to relate the soil amplification to both $V_{S,30}$ and f_0. In this case, f_0 values were directly derived from the numerical amplification functions.

The (log) regression model adopted in this study is represented by the following general equation:

$$\ln Y = a + b_1 \ln X_1 + b_2 \ln X_2 + \cdots\cdots + b_i \ln X_i + \varepsilon \qquad (6)$$

where Y indicates the soil amplification factor (i.e., *Fa*, *Ca*, *Cv*, or *SR*(T)), X_i are the predictors (i.e., $V_{S,30}$ and f_0), and ε is the residual between data and model.

Figures 4 and 5 displays the average amplification factors and regression curves obtained for the same PGA classes considered in Fig. 3, 0.05 g < PGA ≤ 0.15 g and PGA > 0.35 g. The relation between *SR*(T) and $V_{S,30}$ is presented for 4 spectral periods, 0.01 s (≈ PGA), 0.3 s, 1.0 s, and 3.0 s. The goodness of fit is evaluated by analyzing the standard deviation of the residual, $\sigma_{\ln(Y)}$, and the coefficient of multiple determination, $R^2_{\ln(Y)}(\text{adj})$, adjusted for its associated degrees of freedom. $R^2_{\ln(Y)}(\text{adj})$ is a measure of the effectiveness of the model in predicting the dependent variable. This statistic can take on any value less than or equal to 1, with a value closer to 1 indicating a better fit. For the ground shaking classes considered in Fig. 4 and Fig. 5, the values of $\sigma_{\ln(Y)}$ and $R^2_{\ln(Y)}(\text{adj})$ are presented in Fig. 6 where they are compared with those obtained by adding f_0 to the model in $V_{S,30}$. It should be observed that the values of $R^2_{\ln(Y)}(\text{adj})$ tend decrease along with PGA level while those of $\sigma_{\ln(Y)}$ do not show significant variations. This may depend on either the accelerograms used in input or the different behavior of soils at different shaking levels.

Comparing panels in Fig. 4 and Fig. 5, and analyzing Fig. 6 shows that the best correlations between the average soil amplification and $V_{S,30}$ are found when frequency-independent amplification factors are adopted. Considering response spectral ratios (bottom panel of Fig. 3 and Fig. 4), indeed, $V_{S,30}$ is effective in predicting the soil amplification only at medium-to-long spectral periods (i.e., 1.0 s and 3.0 s) where $R^2_{\ln(Y)}(\text{adj})$ is around 0.3 to 0.4 (or greater) and $\sigma_{\ln(Y)}$ does not exceed 0.3. For short-period motions (i.e., 0.01 s and 0.3 s), *SR*(T) and $V_{S,30}$ appear poorly correlated (significant data dispersion). This is particularly evident when strong ground-motions (i.e., PGA > 0.25 g) are applied at the base of the soil columns. In such cases, the correlation coefficient can be as low as 2% and $R^2_{\ln(Y)}(\text{adj})$ values are close to zero (see Fig. 6b), indicating that the predictive power of $V_{S,30}$ is low or nonexistent. A comparison of the values of $\sigma_{\ln(Y)}$ and $R^2_{\ln(Y)}(\text{adj})$ obtained for frequency-independent factors indicates that $\sigma_{\ln(Fa)}$ is generally lower than $\sigma_{\ln(Ca)}$ but it is greater than $\sigma_{\ln(Cv)}$. For example, for PGA levels comprised

between 0.05 g and 0.15 g (Fig. 4), $\sigma_{\ln(Fa)}$ (= 0.24) is approximately 30% lower than $\sigma_{\ln(Ca)}$ (= 0.34) while $R^2_{\ln(Fa)}$(adj) (= 0.45) is 9% greater than $R^2_{\ln(Ca)}$(adj) (= 0.41g). Differences between the values of $\sigma_{\ln(Fa)}$ and $\sigma_{\ln(Ca)}$ are close to those observed between $\sigma_{\ln(Fa)}$ and $\sigma_{\ln(Cv)}$ but, in this case, $\sigma_{\ln(Cv)}$ (= 0.17) is lower. Analogous observations can be made comparing $R^2_{\ln(Fa)}$(adj) and $R^2_{\ln(Cv)}$(adj). However, it is worth noting that for PGA levels greater than 0.25 g, $R^2_{\ln(Ca)}$(adj) drops below 0.1, indicating the low predictive power of $V_{S,30}$ when the amplification factor is defined based on acceleration spectrum intensity values calculated for narrow period intervals (i.e., 0.1-0.5 s).

Including f_0 in the regression model significantly improve the prediction of the soil amplification, as indicated by the lower values of $\sigma_{\ln(Y)}$ and the higher values of $R^2_{\ln(Y)}$(adj) (see Fig. 6). This confirms results by Barani et al. (2008) showing that f_0 is more informative than $V_{S,30}$ and that a model in both $V_{S,30}$ and f_0 yields a lower error in predicting the soil amplification than using $V_{S,30}$ only.

EXAMPLE SHAKING MAPS

In order to verify the reliability of the amplification factors calculated in this study, example shaking maps are elaborated for the destructive earthquake occurred in L'Aquila on April 6, 2009 with magnitude M_w = 6.3. Figures 7 and 8 display ground shaking maps for PGA and 5%-dampded 3.0 s spectral acceleration, S_a(3.0 s), respectively. Specifically, maps in the left column do not account for instrumental data recorded during the earthquake. They simply derive from interpolation of corrected ground-motion values predicted by the attenuation equation by Akkar and Bommer (2007). In the right column, instead, predicted ground-motion values are combined with instrumental measurements of shaking. The rows corresponds to maps derived from the application of different soil amplification factors, all calculated as a function of $V_{S,30}$. It should be remembered that the official maps (first row) are based on the soil coefficient values proposed by Borcherdt (1994). Maps based on the application of frequency-dependent correction factors, $SR(T)$, are not developed since the effectiveness of the model in $V_{S,30}$ in predicting $SR(T)$ was found to be very low at short spectral periods.

Before analyzing Fig. 7 and Fig. 8 separately, it is worth observing that including the information from instrumental data can modify substantially the ground-motion distribution. This is particularly evident in Fig. 8 where the maps on the left side underestimate the recorded motions by a factor of 2.

Focusing on the PGA maps (Fig. 7), it is evident that the application of the Borcherdt coefficients provides ground-motions that are lower than those recorded. Differences can be as high as 20% g. On the other hand, maps resulting from the application of *Fa* and *Ca* values are a reliable picture of the ground shaking recorded at different seismic stations. However, a careful analysis of these maps reveals that the use of the *Ca* values in conjunction with the attenuation equation of Akkar and Bommer (2007) tend to slightly overestimate (5 to 10%) the observed ground-motions. This can be deduced by comparing maps obtained with and without the use of instrumental measurements. Near the epicenter, indeed, the map on the right column presents lower PGA values than that on the left, indicating a slight overestimation of the measured PGA values.

As observed previously, S_a(3.0 s) maps derived from the application of the soil coefficients to the rock ground-motion predicted by the attenuation equation (left column of Fig. 8) underestimate significantly the measured shaking level. This indicates that, for long-period motions, the effect of the amplification factor on the predicted shaking is of secondary importance if compared to the influence of the attenuation equation. This also explains why the maps in the left column do not present significant differences. Once again, however, the best agreement with recorded data is reached applying the *Fa* factor values. Therefore, following the comparison with instrumental data and following results from regression analyses, the application of a single frequency-independent amplification factor may be considered preferable than the use of two separate coefficients for short- and long- period motions. The values of *Fa* used to develop the maps in Fig. 7 and Fig. 8 are presented in Table 2. Note that, although a correct use of the predictive model is limited to $V_{S,30}$ values comprised between 369 and 1227 m/s, results are extrapolated down to $V_{S,30}$ = 300 m/s. Moreover, the *Fa* values corresponding to $V_{S,30} \geq 1000$ m/s are assumed equal to 1 since the soil data set used to calibrate the predictive model lacks of a sufficient number of firm-to-hard rock sites and, consequently, the model may overestimate the ground-motion amplification for very high $V_{S,30}$ values.

Table 2. Values of Fa as a function of $V_{S,30}$ and rock shaking level.

$V_{S,30}$	ROCK SHACKING LEVEL (g)				
(m/s)	PGA ≤ 0.05	0.05 < PGA ≤ 0.15	0.15 < PGA ≤ 0.25	0.25 < PGA ≤ 0.35	PGA > 0.35
1000	1.0	1.0	1.0	1.0	1.0
800	1.27	1.25	1.37	1.54	1.35
700	1.31	1.32	1.42	1.57	1.40
600	1.37	1.40	1.49	1.60	1.45
500	1.43	1.50	1.57	1.65	1.52
400	1.52	1.63	1.68	1.70	1.60
300	1.54	1.81	1.82	1.78	1.72

SUMMARY AND CONCLUSIONS

This study has presented the calibration of soil amplification factor values for application to real-time (or quasi real-time) ground-motion scenarios in Italy using ShakeMap® (Wald et al., 2003). To this end, 1D equivalent-linear dynamic analyses were performed to investigate the response of a hundred of soil columns with different properties. Predictive relations between the soil amplification, quantified by frequency-dependent and -independent factors, and $V_{S,30}$ were then established for different ground-motion levels. Following suggestions of Barani et al. (2008), regression analyses were also performed adding f_0 to the model in $V_{S,30}$.

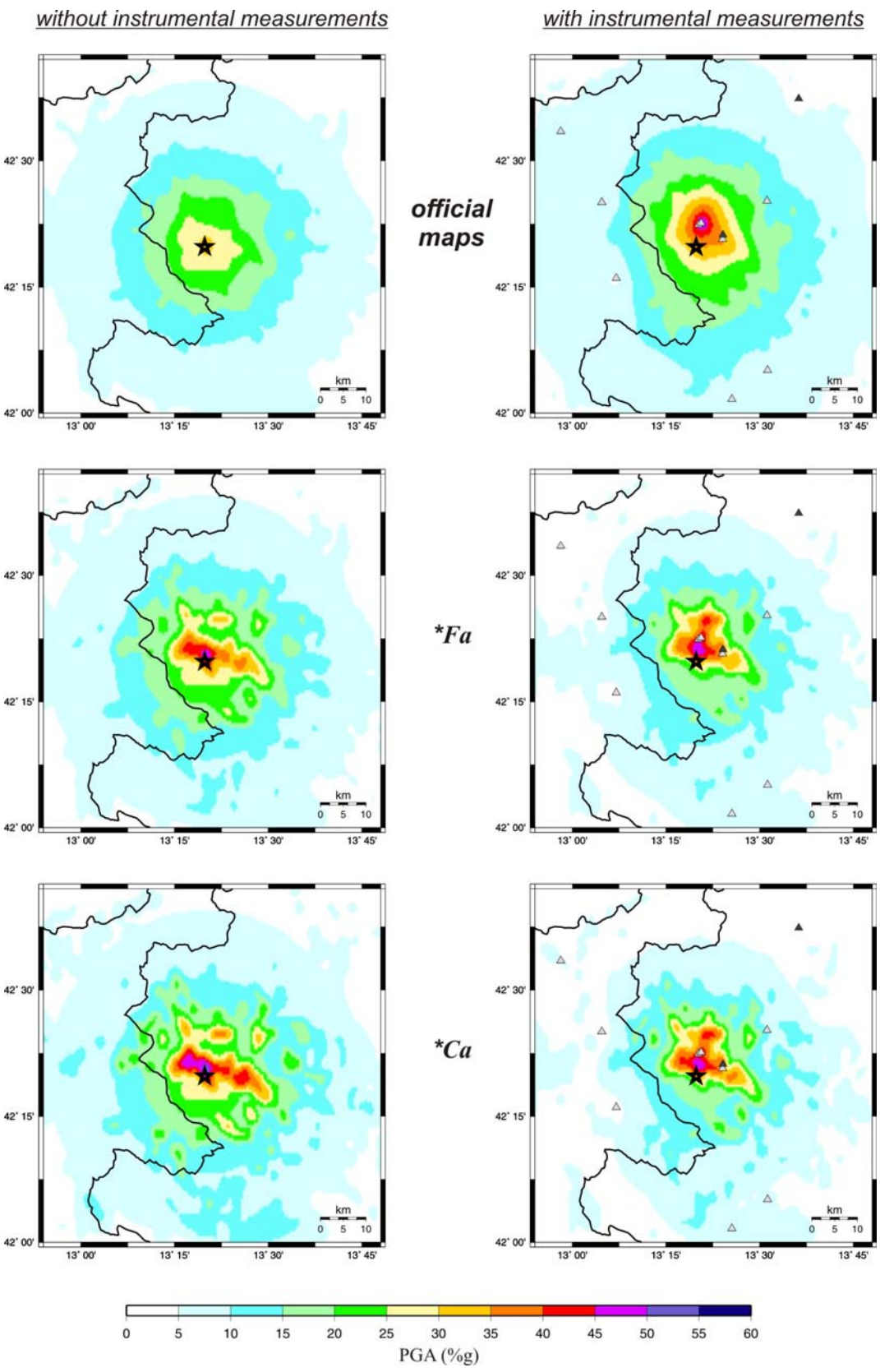

Fig. 7. Comparison between the official PGA map relative to the April 6, 2009 L'Aquila earthquake (first row; http://earthquake.rm.ingv.it/shakemap/shake/index.html) and PGA maps derived from the application of the amplification factors calibrated in this study (second and third rows). Triangles are seismic stations. Earthquake epicenter is indicated by a black star.

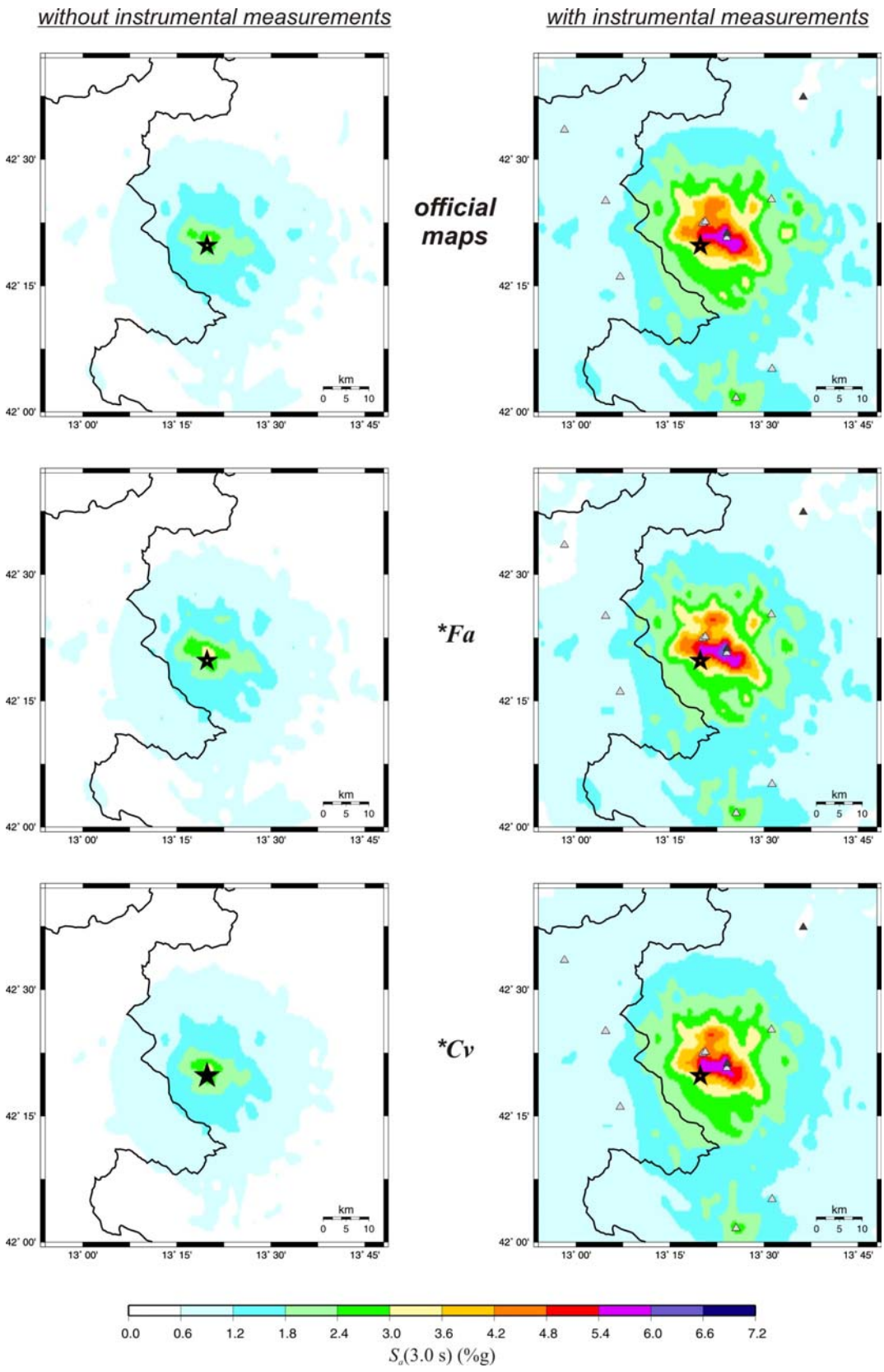

Fig. 8. Comparison between the official S_a(3.0 s) map relative to the April 6, 2009 L'Aquila earthquake (first row; http://earthquake.rm.ingv.it/shakemap/shake/index.html) and S_a(3.0 s) maps derived from the application of the amplification factors calibrated in this study (second and third rows). Triangles are seismic stations. Earthquake epicenter is indicated by a black star.

We found that the effectiveness of the $V_{S,30}$ model in predicting the soil amplification depends on the level of shaking. Specifically, the predictive power tends to decrease with increasing shaking level. Moreover, the effectiveness of the predictive model depends on the parameter adopted to quantify the soil amplification. In particular, our study revealed that if the amplification factor is defined in terms of response spectral ratio, $SR(T)$, the predictive power of $V_{S,30}$, quantified by $R^2_{\ln(Y)}(\text{adj})$, varies substantially with T. It is low (or null) for high frequency response and increases at medium-to-long spectral periods. For this reason, the use of a frequency-independent amplification factor is preferable. In this study, we considered two possible definitions, both based on the ratio of the (acceleration or pseudo-velocity) response spectrum intensity at the surface to the response spectrum intensity at the rock outcrop. In one case a single amplification factor, *Fa*, is defined while in the other distinction is made between short- and long-period motions. In this second case, results of regression analyses show that, for seismic motions characterized by high PGA levels (e.g., PGA > 0.25 g), the correlation between the soil amplification factor for short-period motions, *Ca*, and $V_{S,30}$ is poor. Although this behavior was not observed for long-period motions, the application of a single frequency-independent factor appears preferable for future application of ShakeMap® (Wald et al., 2003) in Italy. This is also justified by comparison with instrumental measurements of shaking. Indeed, the application of the F_a values to define updated shaking maps for the April 6, 2009 L'Aquila earthquake (M_w = 6.3) yielded a ground-motion geographical distribution that agrees better with experimental data recorded during the event. If compared to the official maps, which are based on the application of the amplification factor values calibrated by Borcherdt (1994) using U.S. soil data, the new maps indicate an improvement in the reliability of the ground-motion distribution, particularly for short-period motions.

As a further important result from this study, it is worth remarking the importance of using the soil fundamental frequency for the characterization of the ground-motion amplification in both linear and nonlinear soils. Although $V_{S,30}$ is currently adopted as standard parameter for site classification in ShakeMap®, future implementation of f_0 maps will reduce the error in predicting the soil amplification, increasing the reliability of the shaking maps.

Future studies will investigate the influence of accelerograms on the variability of the amplification factor values and will examine in depth the effect of soil nonlinearity on the stability of regression results. Moreover, new soil profiles will be added to the data set and updated amplification factor values will be released with the aim of providing a portrayal of the ground shaking as close as possible to that produced following an earthquake.

ACKNOWLEDGMENTS

We are grateful to Enzo Zunino (expert technician working at the Laboratory of Seismology of the University of Genoa) for his precious suggestions during the selection of ground-motion records.

REFERENCES

Akkar, S. and J.J. Bommer [2007], "Empirical prediction equations for peak ground velocity derived from strong motion records from Europe and the Middle East", Bull. Seism. Soc. Am., No. 97, pp. 511-530.

Ambraseys, N., P. Smit, R. Sigbjornsson, P. Suhadolc and B. Margaris [2002], "Internet-site of European strong motion data", European Commission, Research-Dictorate General, Environment and Climate Programme.

Barani, S., R. De Ferrari, G. Ferretti and C. Eva [2008], "Assessing the effectiveness of soil parameters for ground response characterization and soil classification", Earthquake Spectra, No. 24, pp. 565-597.

Bazzurro, P. and C.A. Cornell [2004], "Ground-motion amplification in nonlinear soil sites with uncertain properties", Bull. Seism. Soc. Am., No. 94, pp. 2090-2109.

Borcherdt, R.D. [1994], "Estimates of site-dependent response spectra for design (methodology and justification)", Earthquake Spectra, No. 10, pp. 617-653.

Building Seismic Safety Council [2003], "NEHRP Recommended provisions for seismic regulations for new buildings and other structures", Federal Emergency Management Agency – FEMA, Report No. 450, Washington DC, USA.

Choi, Y. and P. Stewart [2005], "Nonlinear site amplification as function of 30 m shear wave velocity", Earthquake Spectra, No. 21, pp. 1-30.

Comitè Europèen de Normalisation [2003], "prENV 1998-1 – Eurocode 8: Design of structures for earthquake resistance. Part 1: General rules, seismic actions and rules for buildings", Draft No. 4, Brussels, Belgium.

Foti, S., D. Lo Presti, O. Pallara, M. Rainone and P. Signanini [2002], "Indagini geotecniche e geofisiche per la caratterizzazione del sito di Castelnuovo Garfagnana", Rivista Italiana di Geotecnica, No. 3, pp. 42-60.

Gruppo di Lavoro MPS [2004], "Redazione della mappa di pericolosità sismica prevista dall'Ordinanza PCM 3274 del 20 marzo 2003", Rapporto conclusivo per il dipartimento di

Protezione Civile, INGV, Milano – Roma, aprile 2004, 65 pp. + 5 appendici, http://zonesismiche.mi.ingv.it/elaborazioni/

Housner, G.W. [1952], "Spectrum intensities of strong motion earthquakes", *Proc. Symposium on earthquake and blast effects on structures*, EERI, Oakland, California, USA, pp. 20-36.

Idriss, I. M. and J.I. Sun [1993], "User's manual for Shake91: A computer program for conducting equivalent linear seismic response analyses of horizontally layered soil deposits", Center for geotechnical modeling, Dept. of Civil and Environmental Engineering, University of California, Davis.

Makdisi, F.I. and H.B. Seed [1978], "Simplified procedure for estimating dam and embankment earthquake-induced deformations", Journal of the Geotechnical Engineering Division, ASCEE, No. 104, pp. 849-867.

Meletti, C. and V. Montaldo [2007], "Stime di pericolosità sismica per diverse probabilità di superamento in 50 anni: valori di a_g", Progetto DPC-INGV S1, http://esse1.mi.ingv.it/d2.html/

Ministero delle Infrastrutture e dei Trasporti [2008], "Norme tecniche per le costruzioni – NTC, D.M. 14 Gennaio 2008", Supplemento ordinario alla Gazzetta Ufficiale No 29, 4 Febbraio 2008.

Pitilakis, K.D., C. Gazepis and A. Anastasiadis [2006], "Design response spectra and soil classification for seismic code provisions", *Proc. ETC-12 Workshop*, January 20-21, Athens.

Rey, J., E. Faccioli and J.J. Bommer [2002], "Derivation of design soil coefficients (S) and response spectral shapes for Eurocode 8 using the European Strong-Motion database", Journal of Seismology, No. 6, pp. 547-555.

Roure, F., P. Casero and R. Vially [1991], "Growth processes and melange formation in the southern Apennines accretionary wedge", Earth and Planetary Science Letters, No. 102, 395-412.

Schnabel, P.B., J. Lysmer and H.B. Seed [1972], "SHAKE: a computer program for earthquake response analysis of horizontally layered sites", Report No. UCB/EERC-72/12, Earthquake Engineering Research Center, University of California, Berkeley, 92p.

Seed, H.B. and I.M. Idriss [1970], "Soil moduli and damping factors for dynamic response analyses", Report No. EERC 70-10, Earthquake Engineering Research Center, University of California, Berkeley.

Seed, H.B., R.T. Wong, I.M. Idriss and K. Tokimatsu [1986], "Moduli and damping factors for dynamic analyses of cohesionless soils", Journal of Geotechnical Engineering, No. 112, pp. 1016-1032.

Sun, J.I., R. Golesorkhi and H.B. Seed [1988], "Dynamic moduli and damping ratios for cohesive soils", Report No. EERC-88/15, Earthquake Engineering Research Center, University of California, Berkeley.

Von Thun, J.L., L.H. Rochim, G.A. Scott and J.A. Wilson [1988], "Earthquake ground motions for design and analysis of dams", in *Earthquake Engineering and Soil Dynamics II – Recent Advance in Ground-Motion Evaluation*, Geotechnical Special Publication, No. 20, ASCEE, New York, pp. 463-481.

Wald, D.J., B.C. Worden, V. Quitoriano and K.L. Pankow [2006], "ShakeMap® manual, users guide, and software guide", U.S. Geological Survey, Techniques and Methods 12-A1, http://pubs.usgs.gov/tm/2005/12A01/

Wald, D.J., L. Wald, B. Worden and J. Goltz [2003], "ShakeMap — A Tool for Earthquake Response", U.S. Geological Survey Fact Sheet 087-03.

Working Group ITACA [2008], "Data base of the Italian strong motion data", http://itaca.mi.ingv.it